Volume 1 | Number 1 | Jan 2013 | Pages 1–100

Nanoscale

www.rsc.org/nanoscale

ROYAL SOCIETY OF CHEMISTRY

ROYAL SOCIETY OF CHEMISTRY

www.rsc.org/nanoscale

Precursor Salt Assisted Syntheses of High-Index Faceted Concave Hexagon and Nanorod like Polyoxometalates

Jaya Pal,[a] Mainak Ganguly,[a] Chanchal Mondal,[a] Yuichi Negishi[b] and Tarasankar Pal[a]*

[a]Department of Chemistry, Indian Institute of Technology, Kharagpur-721302, India

[b]Department of Applied Chemistry, Tokyo University of Science, Tokyo 1628601, Japan

E-mail: tpal@chem.iitkgp.ernet.in

Abstract

This paper describes an effective method for precursor salt assisted fabrication and reshaping of two different polyoxometalates $[(NH_4)_2Cu(MoO_4)_2$ (ACM) and $Cu_3(MoO_4)_2(OH)_2$ (CMOH)] of five distinctive shapes through straight forward and indirect routes. Explicit regulation in structural arrangements of ACM and CMOH has been studied in detail with altered precursor salt concentration employing our laboratory developed modified hydrothermal (MHT) method. Morphologically different ACM 3D architectures are evolved with higher molybdate concentration whereas 1D growth of CMOH is observed with increased copper concentration. Interesting morphology transformation of the products has been sorted out employing one precursor salt at a time without using any other foreign reagent. It is proved that giant ACMs become labile in presence of incoming Cu(II) and NH_4^+ ions of the precursor salts. A new strategy for conversion of faceted ACMs (hexagonal plate, circular plate and hollow flower) to exclusive CMOH nanorods through Cu(II) assisted reaction has been adopted. According to thermodynamic augment, the synthesis of rare concave nanostructures with high index facet is still challenging due to their higher reactivity. In this study, concave hexagonal ACM with high index facet {hkl} has been successfully

prepared for the first time from hexagonal ACM through simple etching with ammonium heptamolybdate (AHM), the other precursor salt. Hexagonal ACM corrugates to concave hexagon because of the higher reactivity of {001} crystal plane than that of {010} plane. It has been shown that high index facet exposed concave hexagonal ACM serves as a better catalyst for photodegradation of dye than the other microstructures enclosed by low index facets.

Introduction

Polyoxometalate (POM) is one of the most intriguing inorganic clusters that consists of two or more transition metal oxoanions which are linked by shared oxide ions to form a large, closed three-dimensional giant framework.[1] The significant contemporary interest in POMs reflects their versatile architecture, facile synthesis, material properties, pH dependent fluorescence properties and other innumerable applications in catalysis, medicine, magnetochemistry, material science and electrochemistry.[2-7] Synthesis of POMs (e.g., binary metal oxides containing Mo, W, V, Ta, and a second transition metal such as Cu, Fe, Co, or Ni species) has already fetched noteworthy interest owing to their robust catalytic property in crude oil refining,[8,9] emissive display technology,[10,11] magnetism,[12] sorption,[13] energy storage,[14] water oxidation,[15,16] and aerobic decontamination.[17] Among these materials, molybdenum oxide based material and copper-containing molybdates have received significant attraction mainly because of their catalytic properties and, subsequently, possible applications in solid-state chemistry, ion exchange, and smart windows.[18-20] Although these polyoxo based materials have been well exploited due to its promising applications, only a couple of papers involving their synthetic procedure and chemical property of ammonium copper molybdate [$(NH_4)_2Cu(MoO_4)_2$] and copper molybdenum oxide hydroxide [$Cu_3(MoO_4)_2(OH)_2$] are in existence. A report of ammonium copper molybdate (ACM) preparation in presence of aqueous ammonia has been discussed.[21,22] Zhu et al. reported the

syntheses of curved ammonium copper molybdate and its hierarchical structure from a solution phase approach at room temperature.[13] On the other hand lindgrenite i.e., copper molybdenum oxide hydroxide (CMOH), comparatively rare copper mineral, has received special attention for its unusual crystal structure, Raman spectra, catalytic activity and thermal decomposition behaviour.[23-25] The wonderful architecture,[25,26] magnetic properties[27] and spin frustration[28] etc. of lindgrenite have been accounted out of different synthetic protocols including electrochemical laser ablation.[29] So development of an easy synthetic protocol for these kind of POM structures as well as their catalytic application has been thought to be worthy of importance.

Next development in this area becomes size and shape selective synthesis of metal and metal oxide micro/nanoparticle which has attracted substantial interest in recent years not only due to their shape dependent properties but also due to their wide variety of applications.[30-33] Therefore; exponential growth in the field of controllable synthesis of micro/nanoparticle is of profound interest to the researcher. Many recent efforts have been directed towards the controlled reshaping of particular morphology to enhance their physical/chemical properties and wide variety of applications. To date, several approaches such as redox transformation method,[34] thermal treatment,[35] seed mediated growth,[36] fluorescent light irradiation,[37] tiny halide ions assisted capping,[38] and selective etching[32] etc. have been developed for reshaping to harness a particular morphology. It is understood that reshaping of nanoparticles occur either by site-specific dissolution of nanoparticles or by using controlled overgrowth technique by which one can arrive at high index faceted morphology that shows promising application in catalysis.

Nanocrystals with concave surface rather than flat or convex surface have drawn great interest because of their high index facets. Interestingly, such type of nanocrystals exhibit higher catalytic activity in many reactions due to presence of high density of low-coordinated

atoms, steps, edges and kinks on the high index facets. There are several reports on the synthesis of concave monometallic structures, including Au, Pd, Pt and Rh.[39-42] However, there exists only few works on the synthesis of concave bimetallic systems (Pd-Rh, Pt-Pd and Pd@Au, Fe-Ni).[43-46] Most of them describe enhanced catalytic activity due to the presence of high-index facets in concave nanocube structures. To the best of our knowledge, literature reports describing high-index faceted concave stable hexagonal structures does not exist. So fabrication of such type of active but thermodynamically unfavourable concave hexagonal nanostructures is now a challenging task.

In this present study we have demonstrated a simple, facile, and cost-effective synthetic protocol for the fabrication of two kinds of POM viz. $[(NH_4)_2Cu(MoO_4)_2]$ (ACM) and $[Cu_3(MoO_4)_2(OH)_2]$ (CMOH) only by varying the precursor salts concentration. Then reshaping of different morphologies under MHT has been possible just by employing selective precursor salt which is reported for the first time. Furthermore, using morphologically different three ACM microstructures (hexagonal plate, circular plate and hollow flower) as templates morphology and compositionally analogous CMOH has been obtained independently through Cu(II) assisted reaction. When only hexagonal plate like ACM is employed as template, high index faceted concave hexagonal ACM is obtained through etching with ammonium heptamolybdate (AHM). Finally, all ACM and CMOH microparticles have been exploited to study the photodegradation of congo red solution under visible light irradiation. Concave hexagonal ACM exhibited substantially enhanced photocatalytic activity relative to the other ACMs due to its high index faceted morphology.

Experimental Section

Synthesis of Morphologically Different Shaped $(NH_4)_2Cu(MoO_4)_2$ and $Cu_3(MoO_4)_2(OH)_2$

In a typical synthesis, 10 mL mixture of 0.05 M $Cu(CH_3COO)_2.H_2O$ (CA) and 0.05 M ammonium heptamolybdate (AHM) in the ratio of 1:9, 2:8, 3:7, 8:2 and 9:1 were taken separately in the screw capped test tubes (10.5 cm in length and 1.5 cm in diameter) and heated for 12 h at 80-90 ˚C using a tungsten bulb (100 W) in a closed wooden box (6 inch × 6 inch × 7 inch) (Scheme 1). This experimental reaction set up is known as modified hydrothermal[47] (MHT) (Scheme S1, ESI). From the first three reaction mixtures (CA:AHM = 1:9, 2:8, 3:7) we obtained ACMs with hexagonal plate, circular plate and hollow flower like morphologies. While keeping other reaction parameters fixed, prickly sphere and rod like CMOHs are formed from reactions with a molar ratio of CA:AHM = 8:2 and 9:1, respectively. The as-prepared yellowish-green and light green products were collected by centrifugation and washing; first with distilled water and then with absolute ethanol and dried in vacuum. The experimental conditions for differently shaped ACMs and CMOHs are presented in Table 1.

Cu(II) Assisted Growth of CMOH Nanorods

In a typical synthesis, 0.01 g morphologically different ACMs (hexagonal plate, circular plate, hollow flower) were separately dispersed in 9 mL of 0.05 M CA solution. Then the resulting mixtures were taken in screw capped test tubes and heated by using a 100 W bulb for 12 h under MHT condition. The as-prepared light green products were carefully washed with distilled water and absolute ethanol for several times and dried in vacuum. Here ACMs upon CA treatment gives CMOH nanorods.

AHM Assisted Growth of ACM Concave Hexagonal Plate

Typically, 0.01 g hexagonal plate like ACM was mixed with 9 mL of 0.05 M AHM solution. Then the resulting solution was taken in a screw capped test tube and heated by using a 100 W bulb for 12 h under MHT condition (Scheme 2). The as-prepared yellowish-green products were carefully washed with distilled water and absolute ethanol for several times and dried in vacuum.

Catalytic Degradation of Congo Red

To compare the photocatalytic activities of differently shaped ACMs and CMOHs, congo red solution was used as a model dye. In a typical process, 0.01 g of differently shaped ACM or CMOH microstructures were dispersed separately in an aqueous solution of congo red (50 mL of 2×10^{-5} M) and stirred in the dark for 1 h to establish the adsorption−desorption equilibrium. Then the solution was irradiated under visible light (100 W electric bulb) with continuous stirring. At different time intervals, 3 mL of the reaction mixture was collected and centrifuged to avoid the light scattering due to the interference from the suspended catalyst particles. Then absorption spectra of the supernatant solution were measured using a UV− visible spectrophotometer.

Results and Discussion

X-Ray Diffraction Analysis

The crystallinity and phase structure of the as-prepared ACMs and CMOHs were analyzed by X-ray diffraction study. Fig. 1a-c depicts the XRD patterns of as-synthesized hexagonal plate, circular plate, and hollow flower like ACM microstructures. Fig. S1a, ESI displays the XRD pattern of concave hexagonal ACM, etching product of hexagonal plate like ACM with AHM. All the diffraction patterns correspond to the pure triclinic phase of ammonium copper molybdate $[(NH_4)_2Cu(MoO_4)_2]$, consistent with JCPDS file No. 40-1490. No other peaks are observed, indicating that the as-prepared ACMs are high purity. Fig. 1d,e shows the XRD

patterns of as-synthesized prickly sphere and rod like CMOHs. Again rods like CMOH have also been synthesized by simple addition of CA precursor solution in morphologically different ACM microstructures. Fig. S1b-d, ESI displays the XRD pattern of CMOH rods obtained from hexagonal plate, circular plate, and hollow flower like ACM microstructures. All the diffraction patterns indicate that all the fabricated products are the pure monoclinic phase of crystalline $Cu_3(MoO_4)_2(OH)_2$ (JCPDS file No. 75-1438). As there are no other peaks obtained from molybdenum or copper compounds, so the as-prepared CMOHs are not only highly crystalline but also phase pure.

XPS Analysis

XPS was employed as the quantitative technique to investigate the chemical state and surface atomic composition of ACMs and CMOHs. Fig. 2a shows main core level peaks for Mo3d, C1s, N1s, O1s and Cu2p at binding energies of 233.1, 284.7, 402.4, 530.4, and 933.5 eV, respectively, arising from hollow flower like ACM. Two peaks at 933.5 and 953.5 eV are attributed to the binding energy of $Cu2p_{3/2}$ and $Cu2p_{1/2}$ respectively which matches with the literature value of Cu(II) state (Fig. 2b).[32] Fig. 2c displays the presence of two peaks at 233.1 and 236.2 eV which are assigned to Mo3d.[48] The presence of ammonium ion in $[(NH_4)_2Cu(MoO_4)_2]$ is also confirmed from XPS analysis. Fig. 2d illustrates the peak of N1s at 402.4 eV corresponding to the presence of NH_4^+ ion.[49] Similar results are also found in case of hexagonal, circular, and concave hexagonal plate like ACMs.

Fig. 2e depicts main core level peaks for Mo3d, C1s, O1s, and Cu2p at binding energies of 232.7, 284.6, 530.4, and 933.5 eV, respectively, arising from CMOH nanorods. Two peaks at 933.5 and 953.5 eV are attributed to the binding energy of $Cu2p_{3/2}$ and $Cu2p_{1/2}$ respectively which is in good agreement with the literature value of Cu(II) state (Fig. 2f)[32]. Two peaks at 232.7 and 235.4 eV correspond to the presence of Mo3d (Fig. 2g).[48] We get similar XPS

spectra for CMOH prickly spheres and CMOH rods obtained through Cu(II) assisted reaction.

FESEM and TEM

Morphology and structure of the as-synthesized ACMs and CMOHs were investigated by FESEM analysis (Fig. 3). The morphology of the products is found to be drastically different depending on the precursor's ratios. At 1:9 CA and AHM ratio, the product is found with a hexagonal plate like morphology of length 2.3 μm and width 1 μm (Fig. 3a1, a2). With increase in copper acetate concentration, i.e., at 2:8 CA and AHM ratio, we observed circular plate like ACM with diameter 2.8 μm and width 800 nm (Fig. 3b1, b2). Fig. 3c1, c2 shows that porous flower like morphology of ACM is obtained with 3:7 CA and AHM ratio. High magnification FESEM image displays that each flower is comprised of densely packed nanosheets with a thickness of 100 nm. As a result this architecture becomes highly porous in nature. More intriguingly, each flower contains one hole at the centre. This flower like architectures have average diameter of 3 μm.

Fig. 3d1, d2 reveals that, at 8:2 ratio of CA and AHM, we obtained prickly sphere like CMOH with average diameter of 8 μm. These spheres are comprised of more than thousands of nanorods. Fig. 3e1, e2 shows the FESEM images of rod like CMOH nanostructures, obtained at 9:1 precursor ratio of CA and AHM. Average diameter of these rods is found to be 160 nm.

FESEM image (Fig. 4a-c) reveals that hexagonal plate like ACM bearing with low index facets transformed to concave hexagonal ACM with high index facet after etching with AHM solution. This result indicates that {001} planes of hexagonal plate like ACM are more reactive than from {010} planes. Fig. 4d-f shows the FESEM images of the products obtained after treatment of differently shaped ACMs (hexagonal plate, circular plate and hollow flower) with CA solution. From these FESEM images, it is observed that all three differently

shaped ACMs are converted to rod like CMOH. The formation of CMOH nanorods has also been confirmed from XRD analysis.

To further confirm the morphology of as-obtained ACMs and CMOHs, we have performed TEM analysis (Fig. 5). TEM images (Fig. 5a,b) of the ACMs at precursors ratio CA:AHM = 1:9 and 2:8, illustrating the formation of hexagonal and circular plate like morphology. Fig. 5c shows the flower like morphology of ACM obtained at precursors ratio CA:AHM = 3:7. This TEM image clearly exhibits the presence of central hole of flower. Low magnification TEM analysis (Fig. 5d) demonstrates that prickly spherical morphology of CMOH (precursors ratio CA:AHM = 8:2) consisted of densely packed nanorods. High magnification TEM analysis (Fig. 5e) clearly reveals the presence of nanorods (average diameter 160 nm) in prickly spherical CMOH. Fig. 5f,g shows the low and high magnification TEM images of rod like CMOH (precursors ratio CA:AHM = 9: 1) having average diameter in the range of 160 nm. So TEM images are in good agreement with FESEM images. Fig. S2a, ESI displays a typical TEM image of AHM etched product that contains ACM hexagon with a concave structure. Fig. S2b-d, ESI shows the TEM images of CMOH nanorods, obtained after treatment of differently shaped ACMs (hexagonal plate, circular plate, and hollow flower) with CA solution.

Growth Mechanism

The formation of two POMs (ACM and CMOH microstructures) of varied shapes can easily be achieved by a single step one pot synthetic protocol. Two precursor salts (CA and AHM) are taken at different ratios to observe their effect on the formation of differently shaped ACM and CMOH microstructures. Alteration of reagent proportion for morphology as well as composition tuning from the same reaction mixture has been explored for understanding the structural change and composition variation of the POMs.

At the indicated 1:9 CA and AHM precursor ratio i.e. at low copper salt concentration, we observe the formation of hexagonal plate like ACM. Circular plate like ACM has been obtained at precursors ratio CA:AHM = 2:8. At the intermediate precursor concentration i.e. at 1.5:8.5, we obtain a mixture of products with hexagonal as well as circular plate like microstructures (Fig. S3a, ESI). Further increase of CA concentration (i.e. 3:7 = CA:AHM precursor ratio) causes the formation of flower, still giving ACM composition. To verify the growth process of flower like morphology, the reaction is carried out at an intermediate concentration ratio i.e. 2.5:7.5 = CA:AHM and flower like over growth on the surface of circular plates is observed (Fig. S3b, ESI). Again increase of CA concentration up to 7:3 = CA:AHM causes rupture of flower like morphology and there appears no particular shape of ACM (Fig. S3c-f, ESI). Prickly sphere like CMOH is obtained at 8:2 = CA:AHM precursor ratio. Finally CMOH nanorods are grown from highest CA concentration (at 9:1 = CA:AHM precursor ratio). It implies that higher concentration of CA is suitable for growth of 1D rod like morphology bearing CMOH composition. On the basis of all the above annotations, it is observed that our proposed method is appropriate for manipulating intrinsic growth of two POMs with different shapes and compositions.

The experimental results for the evolution of particle morphology may be viewed from two different angles (i) formation of particles with 3D morphology and (ii) 1D particle growth. In the first case always CA concentration remains below the concentration of AHM whereas in the second case increased CA concentration plays the dominant role for directional (1D) growth.

Careful observation and time dependent FESEM images reveal that low to moderate CA concentration variation evolve spherical/spheroidal particles at the nucleation stage (Fig. S4 a1, b1, ESI). The particles are viewed to bear different sizes. Upon prolonging the reaction time smaller particles help the growth of larger particles by Ostwald ripening (Fig. S4 a1-a4

and b1-b4, ESI). Thus large hexagonal and circular plates like ACMs are formed (Fig. S4 a4, b4, ESI). Still higher concentration of CA (CA : AHM = 3:7) initiates disintegration of particles right from the beginning causing successive hollowing from the central zone of the spheroidal particle (Fig. S4 c1-c4, ESI). The drift of particle from the central zone of the spheroid caused a 50 % size increment resulting in hollow flower like ACM.

At extremely high concentration of CA (CA : AHM = 9:1) 1D morphology is evidenced without any reorganization of particles (Fig. S4 e1-e4, ESI). Somewhat lower concentration of CA (CA : AHM = 8:2) distinctly support the reorganization of the as prepared particles that helps the formation of spherical assembly of rods (Fig. S4 d1-d4, ESI). Formation of spherical assembly of rods and also the distinct rod formation propagate through oriented attachment mechanism surely at higher CA concentration.

CA and AHM Assisted Growth Mechanism

The fabrication of CMOH nanorod and concave hexagonal ACM has been achieved through precursor salt assisted growth approach. Here hexagonal plate, circular plate, and hollow flower like morphologies of ACMs are separately employed as the templates for fabrication of CMOH nanorod. In all cases, rod like CMOH is obtained from a reaction between CA and ACM microstructures (different morphologies) under MHT condition. On the other hand, only hexagonal plate like ACM microstructure becomes corrugated to concave hexagon because of the simple addition of AHM, the other precursor salt. It is found that the other two ACM microstructures (circular plate and hollow flower) are ruptured and no particular morphology is obtained while they react with AHM. But CMOH (prickly spheres and nanorods) remains totally inert towards the action of both the precursor salts viz., CA and AHM.

To understand the effect of CA on the growth of CMOH nanorods from three different ACM microstructures, experiments were performed with another three Cu(II) salts, namely $CuSO_4$,

CuCl$_2$ and Cu(NO$_3$)$_2$. It is observed that all the three Cu(II) salts are equally competent to evolve similar type of CMOH nanorods (Fig. S5, ESI). From this experiment, it can be concluded that Cu(II) ions are responsible for the formation of the CMOH nanorods and anions have no effect. To verify the effect of Cu(II) concentration on the growth of CMOH nanorods, the experiments were performed with low and high concentration of CA. Low concentration (0.01 M) of CA gives prickly spheres where as high concentration (0.1 M) of CA leads to nanorods with smaller length keeping all other reaction condition unaltered (Fig. S6, ESI). So reaction with 9 mL 0.05 M CA provides the best result for the formation of CMOH nanorods. We further investigated the effect of reaction time on the growth of CMOH nanorods from each ACM microstructures. The products are collected at different time intervals such as 2, 5, 8 and 12 h keeping other parameters fixed (Scheme 3). This result proves that the formation of CMOH nanorods from separate ACM microstructure proceeds through similar pathway. When the reaction time is 2 h, spherical assembly of nanorods (i.e., prickly sphere) was found to appear from each ACM microstructure. With the increase of time up to 5 h, microspheres are destroyed and disintegrated from central zone of the sphere. A few nanorods are found to still remain attached together when the reaction time reached 8 h. When the reaction time is further prolonged to 12 h, rod shaped structure clearly emerges out with average diameter of 160 nm. With time 3D architectures of ACMs are disrupted and get separated as individual nanorod which is evident from the time dependent FESEM images (Scheme 3).

Using the three morphologically different ACM microstructures (hexagon plate, circular plate and hollow flower) as templates, we obtained CMOH nanorods in all the cases through Cu(II) assisted reaction. Therefore on the basis of the above experimental observation, it is concluded that Cu(II) ion causes both structure and composition change while differently shaped ACM microstructures are employed. Upon the addition of Cu(II) ions, ACMs react

with Cu(II) ions under MHT condition and produce CMOH [confirmed from XRD measurement (Fig. S1b-d)] along with NH_4OH. The expelled NH_4^+ ion in the supernatant solution is confirmed by a simple chemical test (NH_3 evolution by NaOH). This result demonstrates that all the NH_4^+ ion are completely removed from the ACM moiety by Cu(II) ion assisted reaction. Surprisingly the as-obtained CMOH attains a rod like morphology which is similar to that of CMOH nanorods obtained from the direct reaction between CA and AHM with a molar ratio of CA:AHM = 9:1. So CMOH nanorods are obtained through two different pathways. One of them describes the synthesis of CMOH nanorods straight forwardly in one step using a particular ratio of precursor salts (CA and AHM). Other route prescribes two step indirect procedure rendering compositional change of ACMs employing as-prepared ACMs and CA. Hence one understands the transformation of 3D architecture of ACMs into CMOH nanorods through dismantling.

$$(NH_4)_2Cu(MoO_4)_2 + Cu\,(II) + H_2O \xrightarrow{\text{MHT}} Cu_3(MoO_4)_2(OH)_2 \downarrow + NH_4OH \quad \ldots\ldots\ldots \text{(i)}$$
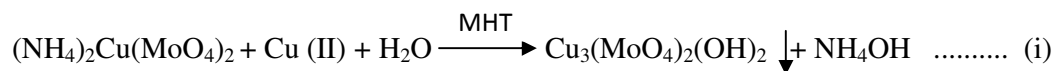
Concave hexagonal ACM, enclosed by high index facet, is obtained through etching with AHM when hexagonal plate like ACM is employed as template (Scheme 2). To elucidate the effect of AHM for the growth of concave hexagonal plate, we have performed the same experiment with Na_2MoO_4. It is found that other Mo(VI) salt cannot be held responsible for etching reaction to fabricate similar type of ACM concave hexagonal plate. But carrying out the same experiment with ammonium acetate or ammonia we obtained concave hexagonal and hollow hexagonal plate like morphology (Fig. S7, ESI). These experimental findings suggest that simple ammonia or NH_4^+ ion of AHM is responsible for etching of hexagonal ACM to concave hexagonal ACM. It has been visualized that the etching property of NH_4^+ ion is most pronounced. But MoO_4^{2-} ion is ineffective to do so. In case of comparative study, the formation of hollow hexagon with ammonia solution exhibits much effective etching than

that of ammonium acetate. The well defined faceted hexagonal morphology is vulnerable to etching with AHM. Then the formation of such typical concave hexagonal morphology indicates that {001} plane of hexagonal ACM is more reactive than that of {010} plane towards etching with AHM.

As a consequence of etching of ACM microparticles, Cu(II) ion passes into the solution which was authenticated by the classical potassium ferrocyanide test. This result once again justify the strong affinity of Cu(II) for free NH_4^+, available from AHM, that helps the dissolution of copper to generate concave hexagonal ACM microstructure. It may be recalled that $[Cu(NH_3)_4]^{+2}$ complex is thermodynamically very stable ($K_f = 1.1 \times 10^{13}$ at 25° C).

So in one case, AHM i.e., one of the precursor salts behaves as etching agent for the formation of concave hexagonal ACM. On the other hand CA (other precursor salt) fetches CMOH nanorods through the disruption of parental ACM building blocks.

Catalytic Activity

Though different organic dyes have influenced our daily life, but due to their toxicity, long persistence, and nonbiodegradable nature, they are hazardous and cause immense damage.[50,51] So the degradation of dyes is a significant concern to build a safe and clean environment. Nowadays, tremendous efforts have been devoted for the degradation of dye molecules, e.g., adsorption tactics, Fenton-like reactions, biological degradation, and photocatalysis, without the formation of any hazardous byproducts.[52-54,32] Among these techniques, photocatalytic degradation of dye molecules has drawn more attention as this method is eco-friendly, reproducible and does not need skilled personnel.

Although POMs have been studied as a cheap photocatalyst for removal of organic dyes, but there are two main disadvantages of these types of photocatalysts. The main disadvantage is their low surface area and second one is the difficulty in recovering them from solution.[55,56] To overcome these problems, researchers have focused incorporation of POMs with

supporting materials, such as TiO$_2$, ZrO$_2$, SiO$_2$ etc.[55-60] But in most cases, POMs exhibits low

visible light photocatalytic activity and might need oxygen as oxidant, an optimum pH

condition or presence of ultrasonic waves. So design and fabrication of water insoluble POM-

based materials for visible light active phtocatalyst is now a challenging task.

Catalytic activity of the differently shaped ACMs and CMOHs were tested for congo red

degradation in presence of visible light. Here we demonstrate for the first time visible light

induced photocatalytic degradation of congo red with water insoluble ACMs and CMOHs. In

the proposed method there is no need of oxygen flow or ultrasonic waves or pH maintenance

for the photocatalytic degradation. Comparative analyses for photodegradation of congo red

solution by various other reported water insoluble POM-based materials[55-60] have been

presented in Table S1, ESI which also includes our best suited concave hexagonal plate like

ACM catalyst. For the catalytic study, 0.01 g of differently shaped ACMs and CMOHs were

added to 50 mL of 2×10^{-5} M congo red solution. Before illumination, the mixture was

allowed to stand under dark condition for 1 h to establish adsorption−desorption equilibrium.

Then the mixture was stirred in presence of visible light (in front of 100 W bulb, under water

coated condition) and 3 mL of the mixture was withdrawn at different time interval and

centrifuged immediately. Absorbance spectra of the supernatant were measured by using

UV−visible spectrophotometer.

Fig. 6a-c displays the extent of photodegradation of congo red solution with respect to time

using ACM hexagonal plate, circular plate, and hollow flower as catalyst. Congo red solution

completely degraded in 28, 35 and 21 min with ACM hexagonal plate, circular plate and

hollow flower respectively. So, the photodegradation ability of differently shaped ACMs

towards congo red degradation follows the sequence: hollow flower (c) > hexagonal plate (a)

> circular plate (b). From literature it is known to us that $\{1\bar{1}1\}$ facets are more reactive than

$\{001\}$, $\{010\}$, and $\{101\}$ facets.[61] So $\{1\bar{1}1\}$ facet dominant ACM hollow flower becomes

more efficient catalyst than {001}/ {010} faceted hexagonal plate and circular plate with {101} facet (Fig. S8a-d, ESI). Now we have performed the same catalytic experiment with concave hexagonal ACM (Fig. 6d). It is observed that concave hexagonal ACM exhibits highest catalytic activity compared to the other three ACMs which implies that high index {422} facets are responsible for such enhanced photocatalytic activity than any other ACMs without high index facets (Fig. S8e, ESI). These high index faceted structures would give much more active sites as atomic steps, edges and kinks at the surface of the concave hexagonal ACM and thus improve the catalytic activity. The plots lnA vs. time (min) for differently shaped ACM catalysts show straight line having negative slopes (Fig. 6e). The values of rate constant for hexagon, circular plate, hollow flower and concave hexagon like ACMs (0.01 g) are 0.0561, 0.0448, 0.0641 and 0.1209 min^{-1} respectively.

The photocatalytic degradation of congo red solution by using different CMOHs are presented in Fig. 7a, b. It is observed that complete degradation of congo red dye solution with CMOH rods required 50 min and for prickly sphere like CMOH 80 min keeping all other parameter unchanged. From literature it is known to us that {111} facets are more reactive than {$\bar{1}$01} facets.[61] In our case also {111} faceted CMOH nanorod shows better photocatalytic activity than that of {$\bar{1}$01} faceted prickly sphere like CMOH (Fig. S8f, g, ESI). We have also performed the same catalytic experiments with CMOH nanorods obtained from Cu(II) assisted growth of differently shaped ACMs and it is seen that this CMOH nanorods also takes comparable time to complete degradation of congo red as before. The plots lnA vs. time (min) for differently shaped CMOH catalysts show straight line having negative slopes (Fig. 7c). The values of rate constant for rod and spherical assembly of rod like CMOHs (0.01 g) are 0.0332 and 0.0234 min^{-1} respectively.

A comparison of the photocatalytic activity revealed that the differently shaped ACMs are more active for the photodegradation of congo red solution than differently shaped CMOHs. So our finding demonstrates that ACM serves as a better candidate for photocatalysis.

To support our contention of facet dependent catalysis, BET surface area measurements (Fig. S9, ESI) for all the ACMs and CMOHs were done. The anomalous and inconclusive results further support the facet dependent catalysis. Authentication is revealed from the highest photocatalytic activity of concave hexagonal plate like ACM due to the promotional effect of high index facet even though it bears lower surface area values.

After the end of photocatalytic experiments, the catalysts were separated from the reaction mixture by centrifugation and washed thoroughly with distilled water and ethanol. The XRD (Fig. S10, ESI) and FESEM (Fig. S11, ESI) analyses of the used and dried catalysts were carried out for confirming the stability of the catalysts. The above analysis demonstrates that there is no change in composition and morphology of the catalysts even after the catalysis which suggests that these catalysts are very much sturdy for practical application. The stability of the photocatalysts is further examined by testing the recyclability and it is found that the catalysts are reusable even after 4th consecutive cycles (Fig. S12, ESI).

Conclusion

A simple, surfactantless, trouble-free and cost-effective synthetic protocol has been used to interpret the precisely controlled fabrication of two different kinds of POMs (ACM and CMOH) of varied shapes. Only variable precursor salt proportion helps us to tune the different morphologies of ACM and CMOH. Again structural and compositional modifications of differently shaped ACMs (hexagonal plate, circular plate and hollow flower) have been successfully achieved only by introducing CA precursor salt in the reaction vessel. In this case it has been proved that ACMs uptake extra load of Cu(II) ion which is responsible for morphology change. Thus maximisation of Cu(II) ion loading in ACM leads

to 1D growth evolving CMOH nanorods. On the other hand, high index faceted concave hexagonal ACM microstructure has been obtained through etching of hexagonal plate like ACM with the other precursor salt i.e, AHM. It is also observed that the stability of {010} crystal plane of hexagonal ACM is higher than {001} crystal plane during etching with AHM. All the concerned reactions are either mass action driven kinetics or prompted by heat. Finally, all ACM and CMOH microparticles demonstrate their facet dependent photocatalytic activity toward the degradation of congo red solution under visible light irradiation. High index faceted concave hexagonal ACM exhibits substantially higher photocatalytic activity than the other ACMs.

Acknowledgements

Electronic Supplementary Information (ESI)

Details about chemicals, analytical instruments, HRTEM, BET surface area, SAED patterns, EDX, area mapping analysis, recyclability test and schematic representation for MHT method. XRD, TEM, FESEM images, HRTEM images, nitrogen adsorption-desorption isotherm, SAED patterns, EDX and area mapping analysis.

References:

1. C. L. Hill and G. C. White, *Chem. Rev*., 1998, **98**, 1-2.

2. D. Li, J. Song, P. Yin, S. Simotwo, A. J. Bassler, Y. Aung, J. E. Roberts, K. I. Hardcastle, C. L. Hill and T. Liu, *J. Am. Chem. Soc*., 2011, **133**, 14010–14016.

3. V. Artero, A. Proust, P. Herson, F. Villain, C. Cartier Dit Moulin and P. Gouzerh, *J. Am. Chem. Soc*., 2003, **125**, 11156-11157.

4. K.-F. Aguey-Zinsou, P. V. Bernhardt, U. Kappler and A. G. McEwan, *J. Am. Chem. Soc*., 2003, **125**, 530-535.

5. L. Lisnard, P. Mialane, A. Dolbecq, J. Marrot, J. M. Clemente-Juan, E. Coronado, B. Keita, P. de Oliveira, L. Nadjo and F. Secheresse, *Chem. Eur. J*., 2007, **13**, 3525-3536.

6. F. Ogliaro, S. P. de Visser, S. Cohen, P. K. Sharma and S. Shaik, *J. Am. Chem. Soc*., 2002, **124**, 2806-2817.

7. J. Zhang, J.-K. Goh, W.-T. Tan and A. M. Bond, *Inorg. Chem*., 2006, **45**, 3732-3740.

8. C. S. Song and X. L. Ma, *Appl. Catal., B,* 2002, **41**, 207-238.

9. A. Ivanov, D. Dimitrov and B. Boyanov, *Chem. Eng. J*., 2009, **154**, 189-195.

10. Q. M. Wang and B. Yan, *Mater. Chem. Phys*., 2005, **94**, 241-244.

11. S. Yu, Z. B. Lin, L. Z. Zhang and G. F. Wang, *Cryst. Growth Des*., 2007, **7**, 2397-2399.

12. D. Tripathy, A. O. Adeyeye, C. B. Boothroyd and S. N. Piramanayagam, *Appl. Phys. Lett*., 2007, **101**, 013904.

13. J. Xu, D. Xue and Y. Zhu, *J. Phys. Chem. B,* 2006, **110**, 17400-17405.

14. S. S. Kim, S. Ogura, H. Ikuta, Y. Uchimoto and M. Wakihara, *Solid State Ionics,* 2002, **146**, 249-256.

15. F. Song, Y. Ding, B. Ma, C. Wang, Q. Wang, X. Du, S. Fu and J. Song, *Energy Environ. Sci.*, 2013, **6**, 1170–1184.

16. H. Lv, J. Song, Y. V. Geletii, J. W. Vickers, J. M. Sumliner, D. G. Musaev, P. Kögerler, P. F. Zhuk, J. Bacsa, G. Zhu and C. L. Hill, *J. Am. Chem. Soc.*, 2014, **136**, 9268–9271.

17. J. Song, Z. Luo, D. K. Britt, H. Furukawa, O. M. Yaghi, K. I. Hardcastle and C. L. Hill, *J. Am. Chem. Soc.*, 2011, **133**, 16839–16846.

18. H. W. Liu and L. Tan, *Ionics,* 2010, **16**, 57-60.

19. G. A. Ozin, S. Ozkar and R. A. Prokopowicz, *Acc. Chem. Res.*, 1992, **25**, 553-560.

20. F. Hamelmann, K. Gesheva, T. Ivanova, A. Szekeres, M. Abroshev and U. Heinzmann, *J. Optoelectron. Adv. Mater.*, 2005, **7**, 393-396.

21. J. L. Garin and J. A. Costamagna, *Powder Diffr.*, 1989, **4**, 233-235.

22. J. Costamagna, J. Garin and A. H. Cowley, *J. Solid State Chem.*, 1993, **105**, 567-572.

23. L. D. Calvert and W. H. Barnes, *Can. Mineral.*, 1957, **6**, 31-51.

24. K. Pavani and A. Ramanan, *Eur. J. Inorg. Chem.*, 2005, **15**, 3080-3087.

25. J. Xu and D. Xue, *J. Solid State Chem.*, 2007, **180**, 119-126.

26. A. Moini, R. Peascoe, P. R. Rudolf and A. Clearfield, *Inorg. Chem.*, 1986, **25**, 3782-3785.

27. S. Vilminot, G. Andre, M. Richard-Plouet, F. Bouree-Vigneron and M. Kurmoo, *Inorg. Chem.*, 2006, **45**, 10938-10946.

28. M. P. Shores, B. M. Bartlett and D. G. Nocera, *J. Am. Chem. Soc*., 2005, **127**, 17986-17987.

29. P. Liu, Y. Liang, X. Lin, C. Wang and G. Yang, *ACS Nano,* 2011, **5**, 4748-4755.

30. H. Zhang, M. Jin, Y. Xiong, B. Lim and Y. Xia, *Acc. Chem. Res*., 2013, **46**, 1783-1794.

31. J. Zeng, Y. Zheng, M. Rycenga, J. Tao, Z.-Y. Li, Q. Zhang, Y. Zhu and Y. Xia, *J. Am. Chem. Soc*., 2010, **132**, 8552-8553.

32. J. Pal, M. Ganguly, C. Mondal, A. Roy, Y. Negishi and T. Pal, *J. Phys. Chem. C,* 2013, **117**, 24640-24653.

33. J. Pal, C. Mondal, A. K. Sasmal, M. Ganguly, Y. Negishi and T. Pal, *ACS Appl. Mater. Interfaces,* 2014, **6**, 9173-9184.

34. J. Pal, M. Ganguly, S. Dutta, C. Mondal, Y. Negishi and T. Pal, *CrystEngComm,* 2014, **16**, 883-893.

35. M. B. Mohamed, K. Z. Ismail, S. Link and M. A. El-Sayed, *J. Phys. Chem. B,* 1998, **102**, 9370-9374.

36. N. R. Jana, L. Gearheart, S. O. Obare and C. J. Murphy, *Langmuir,* 2002**, 18**, 922-927.

37. R. Jin, Y. W. Cao, C. A. Mirkin, K. L. Kelly, G. C. Schatz and J. G. Zheng, *Science,* 2001, **294**, 1901-1903.

38. M. Kim, Y. W. Lee, D. Kim, S. Lee, S.-R. Ryoo, D.-H. Min, S. B. Lee and S. W. Han, ACS *Appl. Mater. Interfaces,* 2012, **4**, 5038-5043.

39. M. Rycenga, M. R. Langille, M. L. Personick, T. Ozel and C. A. Mirkin, *Nano Lett.*, 2012, **12**, 6218-6222.

40. W. Niu, W. Zhang, S. Firdoz and X. Lu, *Chem. Mater.*, 2014, **26**, 2180-2186.

41. Z.-C. Zhang, J.-F. Hui, Z.-C. Liu, X. Zhang, J. Zhuang and X. Wang, *Langmuir,* 2012, **28**, 14845-14848.

42. S. Xie, H. Zhang, N. Lu, M. Jin, J. Wang, M. J. Kim, Z. Xie and Y. Xia, *Nano Lett.*, 2013, **13**, 6262-6268.

43. S. Xie, N. Lu, Z. Xie, J. Wang, M. J. Kim and Y. Xia, *Angew. Chem., Int. Ed.*, 2012, **51**, 10266-10270.

44. H. Zhang, M. Jin, J. Wang, W. Li, P. H. C. Camargo, M. J. Kim, D. Yang, Z. Xie and Y. Xia, *J. Am. Chem. Soc.,* 2011, **133**, 6078-6089.

45. L. Zhang, W. Niu, Z. Li and G. Xu, *Chem. Commun.*, 2011, **47**, 10353-10355.

46. N. Moghimi, M. Abdellah, J. P. Thomas, M. Mohapatra and K. T. Leung, *J. Am. Chem. Soc.*, 2013, **135**, 10958-10961.

47. A. K. Sinha, S. Jana, S. Pande, S. Sarkar, M. Pradhan, M. Basu, S. Saha, A. Pal and T. Pal, *CrystEngComm*, 2009, **11**, 1210-1212.

48. N. V. Lebukhova, V. S. Rudnev, P. G. Chigrin, I. V. Lukiyanchuk, M. A. Pugachevsky, A. Y. Ustinov, E. A. Kirichenko and T. P. Yarovaya, *Surf. Coat. Tech.,* 2013, **231**, 144-148.

49. C. Gabler, C. Tomastik, J. Brenner, L. Pisarova, N. Doerr and G. Allmaier, *Green Chem.*, 2011, **13**, 2869-2877.

50. A. Kar, Y. R. Smith and V. Subramanian, *Environ. Sci. Technol.*, 2009, **43**, 3260-3265.

51. W. Ma, J. Li, X. Tao, J. He, Y. Xu, J. C. Yu and J. Zhao, *Angew. Chem., Int. Ed.*, 2003, **42**, 1029-1032.

52. X. Zhuang, Y. Wan, C. Feng, Y. Shen and D. Zhao, *Chem. Mater.*, 2009, **21**, 706-716.

53. A. Georgi, A. Schierz, U. Trommler, C. P. Horwitz, T. J. Collins and F.-D. Kopinke, *Appl. Catal. B: Environ.*, 2007, **72**, 26-36.

54. K. Pazdzior, S. A. Klepacz, S. Ledakowicz, L. J. Sojka, Z. Mrozinska and R. Zylla, *Chemosphere,* 2009, **75**, 250-255.

55. H. Salavati, N. Tavakkoli and M. Hosseinpoor, *Ultrason. Sonochem.*, 2012, **19**, 546–553.

56. S. Tangestaninejad, M. Moghadam, V. Mirkhani, I. Mohammadpoor-Baltork and H. Salavati, *Ultrason. Sonochem.*, 2008, **15**, 815–822.

57. Y. Yang, Y. Guo, C. Hu and E. Wang, *Appl. Catal., A*, 2003, **252**, 305–314.

58. Y. Yang, Y. Guo, C. Hu, Y. Wang and E. Wang, *Appl. Catal., A*, 2004, **273**, 201–210.

59. Y. Yang, Q. Wu, Y. Guo, C. Hu and E. Wang, *J. Mol. Catal. A: Chem.*, 2005, **225**, 203–212.

60. D. Li and Y. Liu, *Adv. Mater. Res.*, 2011, **298**, 96-101.

61. H. Xu, P. Reunchan, S. Ouyang, H. Tong, N. Umezawa, T. Kako and J. Ye, *Chem. Mater.*, 2013, **25**, 405-411.

Figure, Scheme and Table
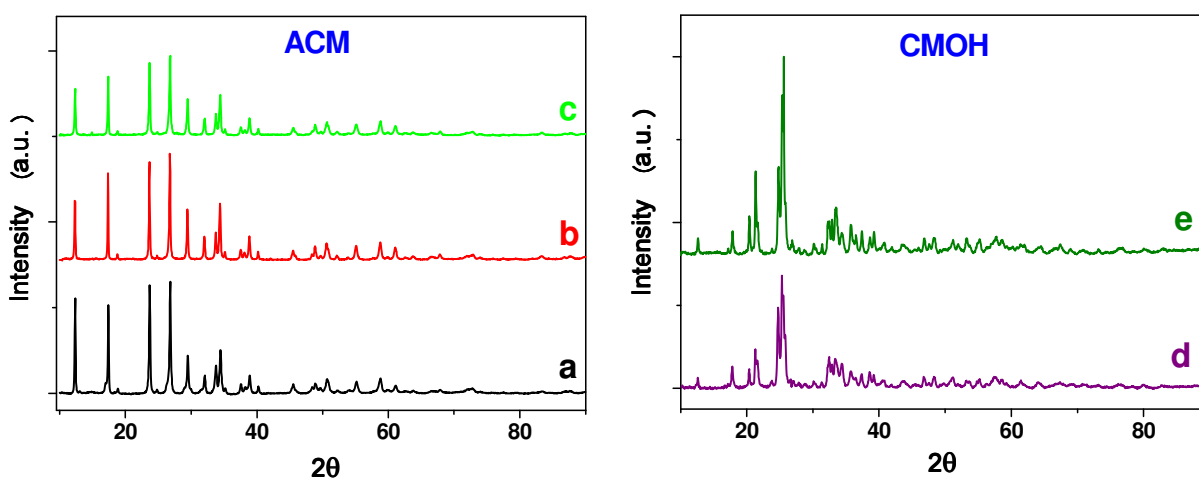
Fig. 1 Curves a-c show the XRD patterns of hexagonal plate, circular plate, and hollow flower like ACM microstructures, respectively. Curves d and e show the XRD patterns of prickly sphere and rod like CMOH microstructures, respectively.
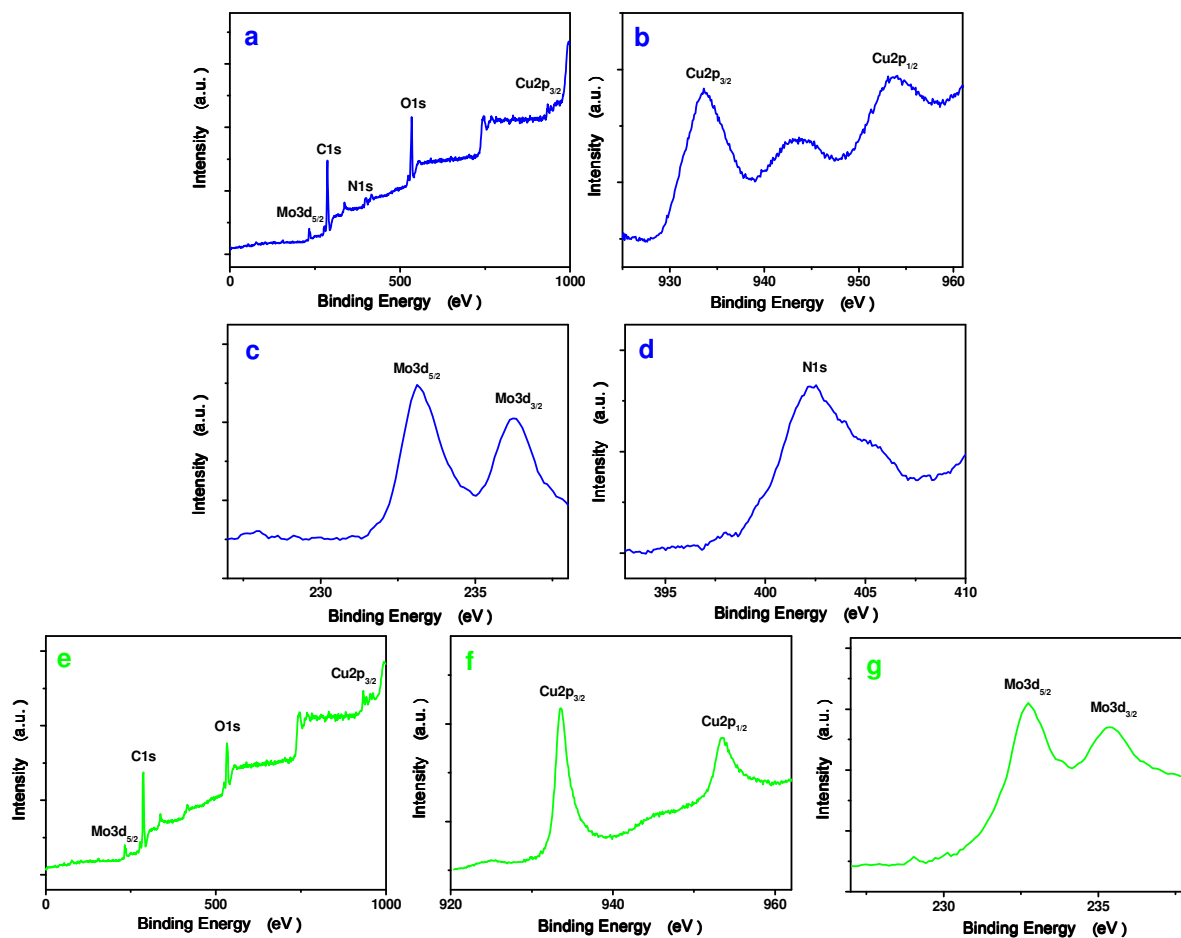
Fig. 2 XPS spectra of hollow flower like ACM microstructure: (a) wide range (b) Cu2p spectrum, (c) Mo3d spectrum, and (d) N1s spectrum. XPS spectra of CMOH nanorod: (e) wide range (f) Cu2p spectrum, and (g) Mo3d spectrum.
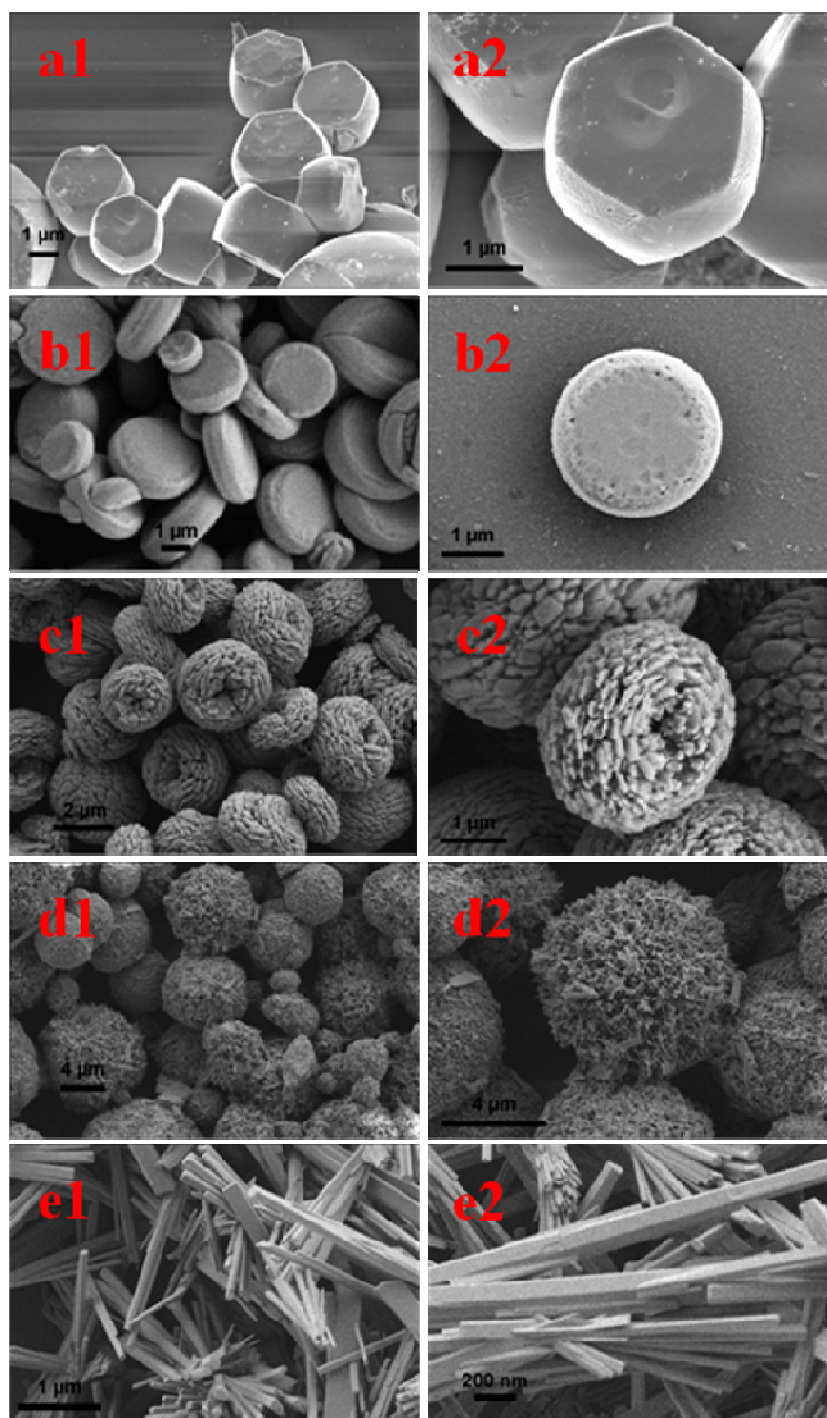
Fig. 3 Low and high magnification FESEM images of (a1 and a2) hexagonal plate, (b1 and b2) circular plate, and (c1 and c2) hollow flower like ACM microstructures, respectively. Low and high magnification FESEM images of (d1 and d2) prickly sphere and (e1 and e2) rod like CMOH microstructures, respectively.
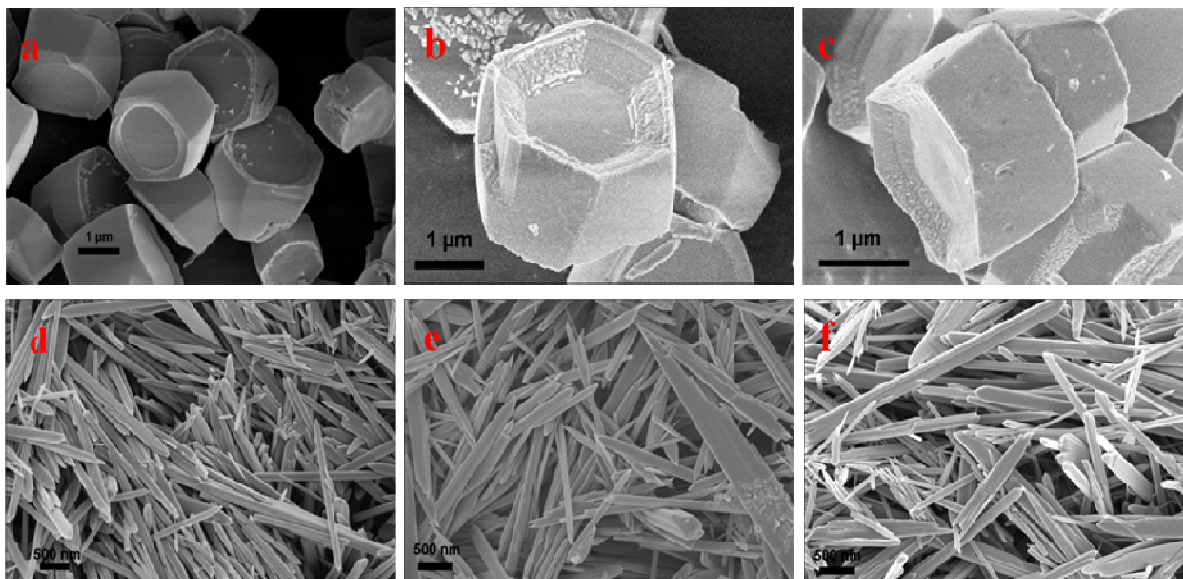
Fig. 4 Low and high magnification FESEM images of (a-c) concave hexagonal plate like ACM after etching with AHM. FESEM images of (d-f) rods like CMOH obtainted from individual reaction of copper acetate with hexagonal plate, circular plate and hollow flower like ACMs, respectively.
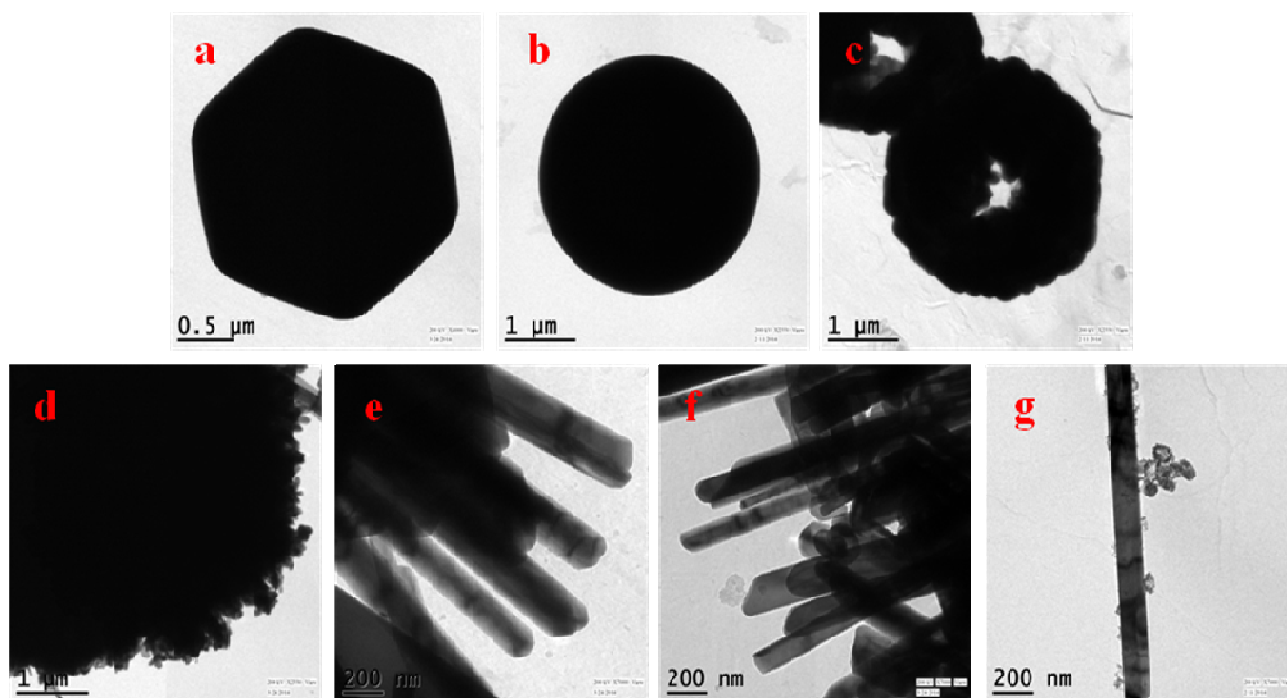
Fig. 5 TEM images of (a) hexagonal plate, (b) circular plate, and (c) hollow flower like ACM microstructures, respectively. Low and high magnification TEM images of (d and e) prickly sphere and (f and g) rod like CMOH microstructures, respectively.
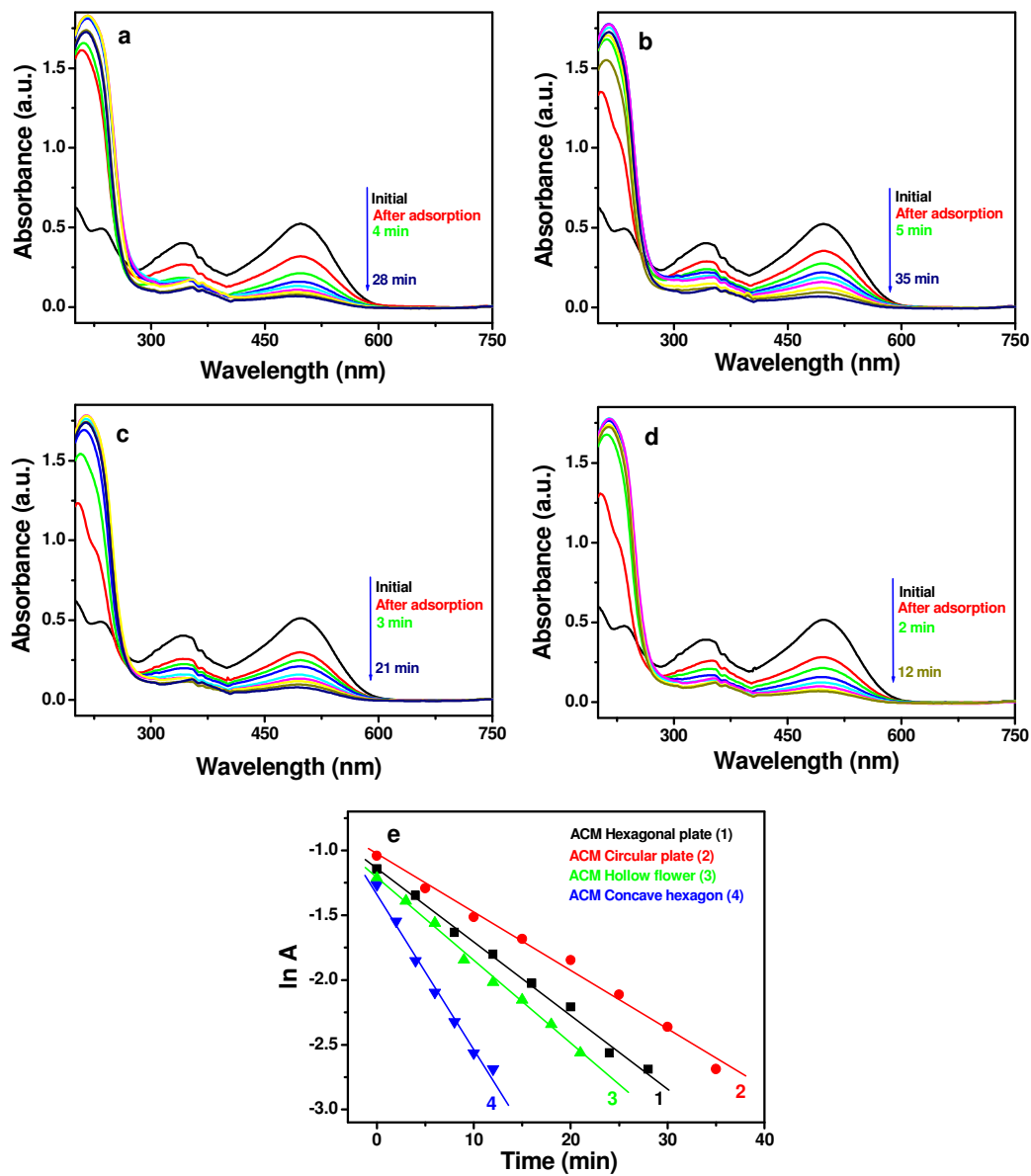
Fig. 6 Photodegradation of congo red solution in presence of visible light by using 0.01g of (a) hexagonal plate, (b) circular plate, (c) hollow flower, and (d) concave hexagonal plate like ACM microstructures, respectively. (e) Corresponding lnA vs time plot.
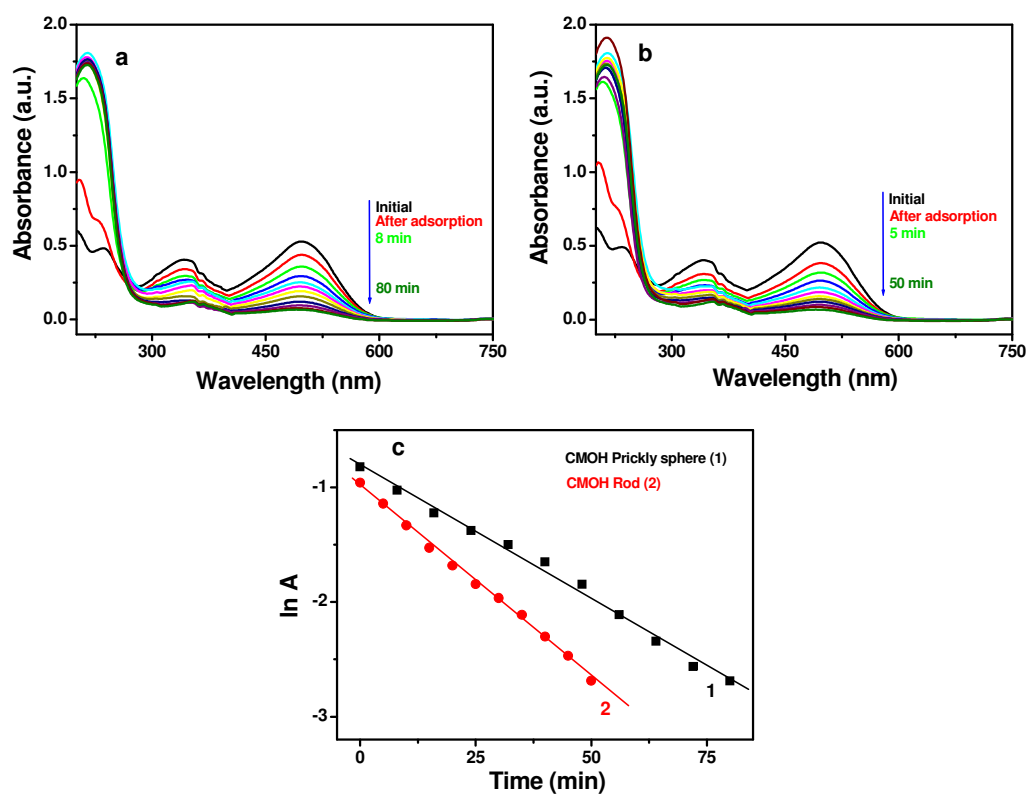
Fig. 7 Photodegradation of congo red solution in presence of visible light by using 0.01g of

(a) prickly sphere, and (b) rod like CMOH, respectively. (c) Corresponding lnA vs time plot.
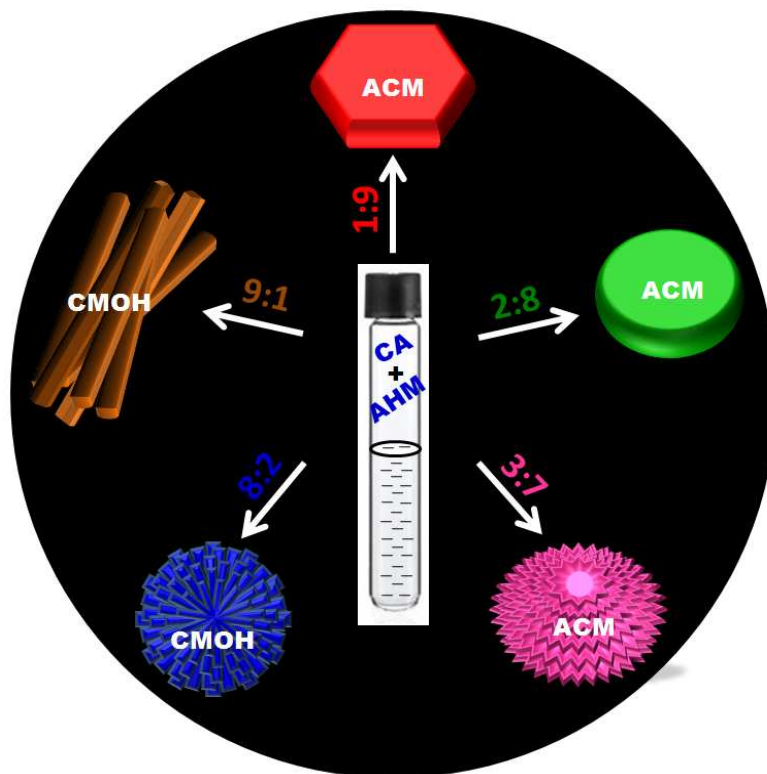
Scheme 1 Schematic representation of morphologycally different ACM and CMOH microstructures obtained by varying the ratio of CA and AHM (CA:AHM = 1:9, 2:8, 3:7, 8:2 and 9:1) under MHT condition for 12 h.
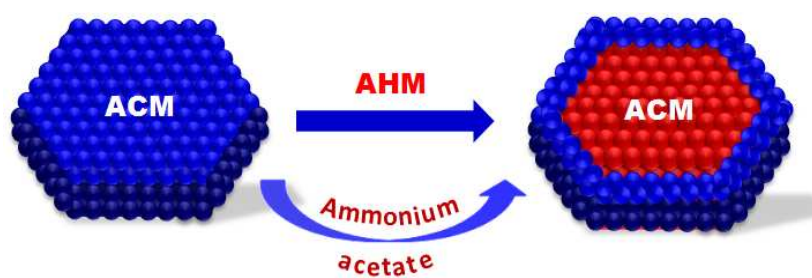
Scheme 2 Schematic representation of formation of concave hexagonal plate like ACM from hexagonal plate like ACM through etching with AHM and ammonium acetate under MHT condition for 12 h.
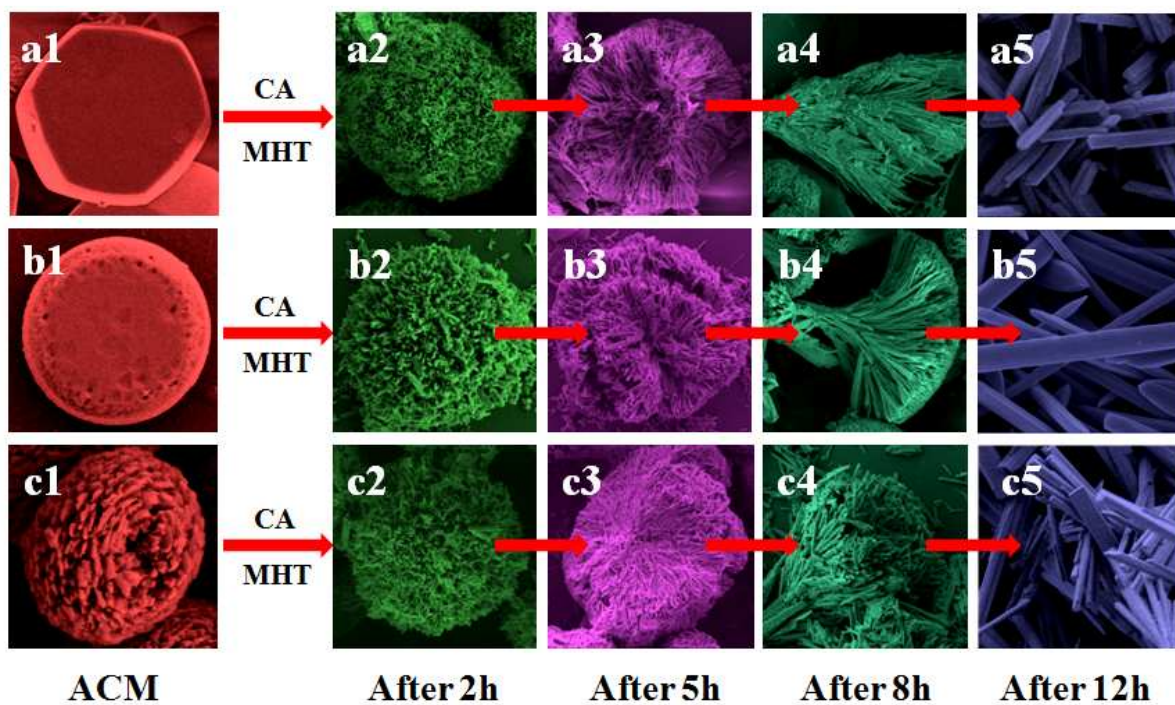
Scheme 3 Schematic representation of time dependent growth process for formation of CMOH nanorods from morphologically different ACM microstructures. CMOH a2, b2 and c2, obtained after 2 h of reaction, a3, b3 and c3, obtained after 5 h of reaction and a4, b4 and c4, obtained after 8 h of reaction and a5, b5 and c5, obtained after 12 h of reaction from (a1) hexagonal plate, (b1) circular plate and (c1) hollow flower like ACM microstructures, respectively.

Table 1. Detail experimental parameters for synthesis of differently shaped ACM and CMOH microstructures.

Composition	Morphology	Precursors Ratio (CA : AHM)	Reaction Time (h)	Condition
ACM	Hexagonal Plate	1:9	12	MHT (100 W Bulb)
ACM	Circular plate	2:8	12	MHT (100 W Bulb)
ACM	Hollow Flower	3:7	12	MHT (100 W Bulb)
CMOH	Prickly Sphere	8:2	12	MHT (100 W Bulb)
CMOH	Rod	9:1	12	MHT (100 W Bulb)

Graphical Abstract

Precursor Salt Assisted Syntheses of High-Index Faceted Concave Hexagon and Nanorod like Polyoxometalates

Jaya Pal,[a] Mainak Ganguly,[a] Chanchal Mondal,[a] Yuichi Negishi[b] and Tarasankar Pal[a]*

[a]Department of Chemistry, Indian Institute of Technology, Kharagpur-721302, India

[b]Department of Applied Chemistry, Tokyo University of Science, Tokyo 1628601, Japan

E-mail: tpal@chem.iitkgp.ernet.in